# Energy Harvesting Potential of Autorotating Turbines

Seth Pearl
*Mechanical Engineering Program*
*SUNY New Paltz, NY*
New Paltz, NY, USA
pearls2@hawkmail.newpaltz.edu

Rachmadian Wulandana
*Mechanical Engineering Program*
*SUNY New Paltz, NY*
New Paltz, NY, USA
wulandar@newpaltz.edu

***Within developed societies energy is extracted from burning fossil fuels for applications such as generating electricity. While this method provides sufficient power to meet the electrical necessities for a wide variety of environments, there are also irreversible effects produced that have a negative impact on the surrounding area. An explored alternative to burning fossil fuels has been through using renewable energy, which makes use of environmental resources in an effort to extract energy from it. The concentration for this research focuses on extracting renewable energy from two different fluids: water and air. The Mechanical Engineering Program of SUNY New Paltz has recently developed a custom water flow tank and a custom air tunnel for use in this research, which will allow for a comparison of generating energy between the two fluids. The method of energy harvesting that will be used is referred to as hydrokinetic energy, which is an environmentally friendly option that involves placing a turbine in the middle of a flowing fluid. As the turbine rotates, the generated mechanical energy is stored in an attached generator, which then converts the mechanical energy into electrical energy. The turbine used in both experiments is a 3D printed cross cylinder bladeless turbine. The bladeless design was implemented as it causes little harm to its surrounding environment as opposed to bladed turbines. Moreover, the designs allow the turbines to be operated on either water or air flow. In the current project, the flow speed was varied in increments while voltage and current were measured. Watt's Law was used to calculate the power generated. Despite the air flow speed surpassing the water flow speed by nearly tenfold, the turbine generated more power when submerged in water for its dense properties.***

***Keywords— Autorotation, renewable energy, bladeless turbines***

## I. INTRODUCTION

Renewable energy is defined as "Any naturally occurring, theoretically inexhaustible source of energy, such as biomass, solar, air, tidal, wave, and hydroelectric power, that is not derived from fossil or nuclear fuel" [1]. Renewable energy is attractive because it is a clean and environmentally friendly alternative to traditional power generation methods that can be used for applications such as electricity and transportation in isolated societies like Brazil [2].

The current project reflects on early progress of an innovative design for power harvesting of kinetic energy from flowing water and air through vortex-induced autorotation phenomena. As is known, hydroelectric power generation currently is still dominated by hydropower technology that relies on the potential energy of water. The hydropower technology requires expensive and massive dams which often cause environmental damage. On the other hand, hydrokinetic energy harvesting has become an attractive topic for investigation as the technology promises a minimum infrastructure requirement and a low impact on freshwater life [3]–[5]. Unlike the wind turbine technology that has reached full maturity and has a historically low average cost of energy [6], the hydrokinetic technology is still developing. In this paper, focus is given to the energy harvesting potential of a sub-category of kinetic energy harvesting known as vortex-induced autorotating objects.

A rotating rotor is properly categorized as autorotating when "one or more stable positions exist at which the fluid flow exerts no torque on the resting body" [7]. An autorotating body requires an initial strong impulse to produce continuous rotational motion. A trivial example of a non-rotating body is when a cylinder fails to rotate about its own long axis when it is fully submerged in a uniform flow. On the other hand, polygonal shapes such as triangular and rectangular prisms can autorotate. The experiment works by Skews on polygonal prisms under air flow showed that triangular and rectangular prisms spin (about its own long axis) faster than polygons with more sides [8]. In the same experiment, Skews also showed that octagonal prisms would not rotate about its long axis, which is expected as the geometry of an octagon prism is close to being a cylinder. The autorotating turbine model introduced in the current work was motivated by the early works on vortex-induced oscillations and autorotation of bodies exposed to fluid flow [9], [10]. In these earlier projects, Delrin plastic cylinders of ~ 6-mm in diameter, with the ratio of length-to-diameter of around unity, were identified to show autorotation about its symmetrical axis parallel to its base. This occurs for a range of Reynolds numbers between ~ 3000 to 4500. In the experiment, the short cylinder was hinged on its centroid and was placed at the middle of an observation channel with a rectangular cross section of 15x15 $cm^2$. The sample was exposed to uniform water flow produced in a water tank.

Built upon the promising results of straight cylinders, the proposed turbine has its shape inspired from an overlapping of two perpendicular cylinders and pinching them about their centroid. The symmetric 3D-printed turbine design has an edge-to edge distance of 5 cm, a mass of 30.5 grams, and an infill density of 10%. This turbine design was chosen for its partially curved surfaces and large flat areas on its four sides. It is expected that these geometrical features would generate sufficient shearing forces and, hence, torque needed for rotation. Additionally, a simple cylinder placed in submerged flowing fluid will naturally stabilize with the longer side perpendicular to the direction of flow. By creating a dual-cylinder design, the turbine will continuously rotate as it always has one cylinder that turns to reach stability. Tests will be performed using both fluids to observe if this design can extract sufficient power at a small scale.

The current design is different from many traditional turbines that capture the kinetic energy of flowing fluid through the drag and lift forces generated on their blades. The turbine model introduced in this work relies on rotational motion induced by vortex shedding trailing on the back of bodies exposed to fluid flow. Vortex-induced vibration (VIV) on bodies subjected to cross flow is ubiquitous in nature and

it often presents concerning matters. The corresponding frequency resonance is typically followed by large lateral oscillations known to cause fatigue and eventual catastrophic failure of the bodies. Typical examples of bodies exposed to fluid flow in industries include pipes and tubes arranged in bundles inside heat exchangers [11], transmission cables [12], towering chimneys [13], and radio antennas [14] that are exposed to flowing air. Interestingly, recent investigation suggests that when the large lateral oscillations can be well controlled and utilized, useful energy harvesting of such mechanisms becomes possible. The Vortex Induced Vibration Aquatic Clean Energy (VIVACE) project is an example of such technology [15]. Principally, the ends of the vibrating tubes of VIVACE are allowed to move in lateral direction (with respect to the flow direction). These "free-to-move" ends are connected to magnetic bars that would move back and forth in between metal coils to create electricity via electromagnetic induction. To generate sufficiently large amounts of electricity, tidal flow and deep river current could potentially be utilized. The energy capture of such vibrating systems can also be facilitated by piezoelectric strips that are either attached on the tubes [16] or being suspended in the vortex-shedding region [17] . The useful energy is produced by the special characteristics of piezoelectric strips that can transform strain energy into electric charges. The turbine discussed in the current paper reflects the vortex-induced rotational modes and rotational oscillation modes, instead of the lateral oscillation modes. Investigations on these modes are lacking and hence warrant attentions. The current turbine design is also unique as it can be operated either in water or in air flow.

In this paper, we will first discuss the turbine model, specification of each flow tank, delving into the specifics of the operating conditions for each flow tank, how the baseline speeds were accumulated, and detailing the methods involved for each experiment while emphasizing the similarities across both apparatuses. The results from both experiments will be discussed next and followed by a conclusion.

## II. METHOD

The 3D-printed turbine model used in this study was designed using SolidWorks CAD software and is shown in Figure 1. Geometrically, the model resembles a combination of two straight cylinders arranged orthogonally and conjoined at its center of gravity. The straight cylinder is unique as it has an equal diameter and length of 5 cm. The resulting shape can be considered as a cube with modified corners. The geometry was inspired by an early work on the vortex-induced oscillations and autorotation potential of a dense cylinder exposed to water flow at low Reynolds numbers [9]. The turbine was made of Polyactic Acid (PLA) with a low 10% infill printing parameter. The dimensions of this model are 5x5x5 $cm^3$, with a mass of 30.5 g and volume of 112.874 $cm^3$. These give an approximate turbine density of 0.270 $g/cm^3$ which is less than the water. Due to the porosity of the model caused by the printing method, the density of the model is only 21% of the density of the PLA. The model was placed about 7 cm below the water surface. The water occupies a little less than 15 cm of chamber depth. The width and length of the transparent observation chamber are 15 and 60 cm, respectively. The top part of both chamber walls are drilled to allow perforated C-bars to be secured on it using screws. The assembly of the motor case was secured using similar C-bars laid out across the chamber.

The water flow tank, as shown in Figure 1, was designed to deliver approximately 12800 gph of water through the 15x15x60 $cm^3$ transparent observation chamber. In order to produce such a flowrate, the system is equipped with a 3-hp centrifugal pump that can be controlled by a Variable Frequency Drive (VFD). The VFD allows the flowing fluid to be controlled either manually or automatically at frequencies ranging from 20 Hz to 55 Hz. The maximum average flow speed that can be achieved is approximately 60 cm/s. A converging chamber was designed at the entrance of the observation chamber to reduce the complexity of the flow and to create uniform flow. The custom made closed-loop flow tank was sponsored by the Vibration Institute and it was constructed as a senior design project within the Division of Engineering of SUNY New Paltz.

In order to gather quantitative data from the autorotating turbine, the axle that was connected to the turbine was coupled to the axle of a 0.5-V DC motor implemented as a generator through a rigid plastic tubing with an internal diameter of 2 mm. The DC motor was then fixated in a 3D-printed enclosure which was fastened to metal brackets above the flowing water. The wire connections from the DC motor were connected to a Dawson Digital Multimeter as shown in Figure 2. The digital multimeter is equipped with a USB connection and compatible software that allows for the collected date to be processed using Excel. The software records measurements at intervals of approximately 0.3 seconds. All measurements were taken over 60 intervals culminating in a total of approximately 20 seconds. Because the multimeter cannot measure voltage, current, and power generated at the same time, tests conducted with this multimeter first measured voltage, then switched to measure current while the flow tank continued to run. The collected data was imported into Microsoft Excel. From there, the absolute values of the measured voltage and current were taken (clockwise and counterclockwise rotations from the turbine yielded negative and positive readings, respectively). Next averages of the absolute value readings were calculated. Finally, oobtaining the power harvested was done using Watt's Law, which states:

$$\bar{P} = \bar{V} \times \bar{I}$$

where $\bar{P}$, $\bar{V}$, and $\bar{I}$ are the average power, average voltage and average current, respectively.

As a result, the power observed is a culmination of separate voltage and current measurements made at the same flow speed. It was assumed that the turbine would not significantly fluctuate in movement patterns at each flow speed increment for prolonged intervals. While the true power generated may not precisely equate to the observed power, it can be assumed that the difference between the true and observed power is insignificant and the correlations between flow speed increments remain valid. Most importantly, the experiment was intended to investigate the potential of autorotation and its trend with the increase of Reynolds numbers and its corresponding average flow speed.

The experiment using air flow was performed using a small custom-made air tunnel that is shown in Figure 2. The laptop, Dawson Digital Multimeter, and methodology previously discussed were kept the same for the air flow measurements. Similar to the water tank, the chamber for the air tunnel has a cross sectional area of about 15x15 $cm^2$ and alength of 45 cm. The turbine was placed 7.5 cm from the front of the chamber and was suspended 6 cm above the floor of the chamber. The air tunnel has a fan that pushes air through

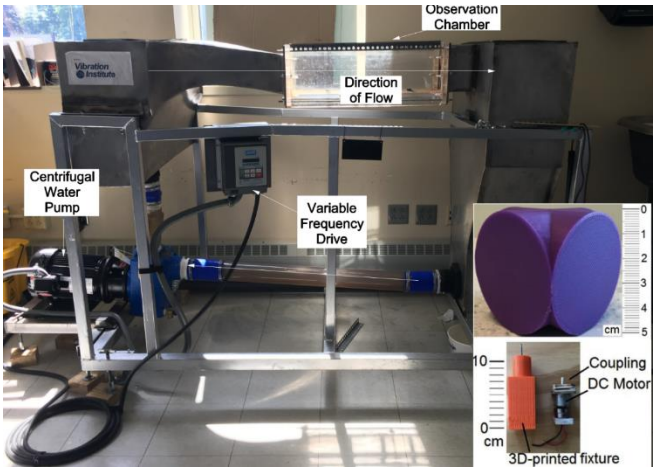


*Figure 1. Water flow tank used for the experiment and the 3D printed turbine model used in the tests. Also shown is the DC motor and water-proof case assembly used in the experiment.*

the brown wooden funnel into the chamber. Measurements were taken from the 12 separate bars on the dial in which the fan speed increases as the knob is turned counterclockwise.

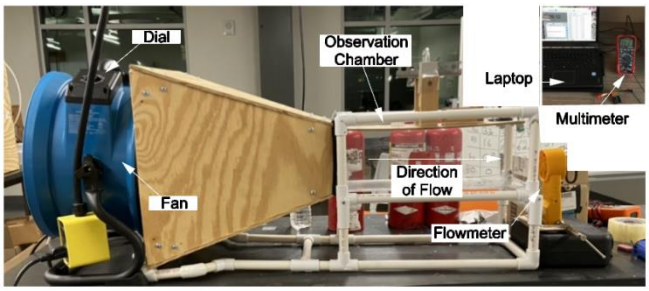


*Figure 2. Air Tunnel with annotations for the fan, knobs (dial), the custom-made transparent observation chamber, and flow meter. The figure on the corner shows the digital multimeter connected to a laptop during the data processing.*

Two experiments were conducted using the air tunnel; RPM and power experiments. While the former was focused on the measurement of RPM using an infra-red tachometer, the latter is similar to the power measurement for the water tank. The tests to measure the RPM were conducted using a turbine model designed for that purpose. For this case, a smooth ball bearing was pressed fit onto the top of the turbine to allow the turbine to rotate freely while the shaft is fixed in its position. The Reynolds number was obtained across all measurements to establish a comparative parameter between the water and air results. To obtain the Reynolds number for the observations the velocity needed to be measured. For the flow tank, to convert the outputting frequency into flow speed (m/s), a flow speed sensor was submerged in the water at varying frequencies. To measure the fan speed in the air tunnel, a flowmeter was positioned at the exit portion of the air tunnel.

## III. Results

Throughout the following discussion below, the flow regimes will be identified by the typical Reynolds number calculated using the following equation:

$$R_e = \frac{\rho V D}{\mu}$$

Here, the ρ,V,D and μ are the fluid density, average fluid speed, turbine diameter of 5 cm, and fluid viscosity, respectively. For water, the density and viscosity are 998 kg/m$^3$ and 9.8x10-4 Pa.s, respectively. While for air, it is assumed that the density and viscosity are 1.2 kg/m$^3$ and 1.2x10-5 Pa.s, respectively.

In order to measure the flow speed of water and air, flow measurement devices were used at varying increments for flow speed data collection. For the water flow tank, a Flow Rate Sensor by Vernier was utilized. The sensor can be used for water flowing at room temperatures with a maximum velocity of 4 m/s. The device's accuracy is ±1%. The water flow speed in the chamber can be varied by adjusting the frequency of the pump using the digital VFD. The flow speed measurements were acquired using Vernier's LoggerPro software. The data then was imported into an Excel file to be further processed. For the air tunnel, a digital flowmeter was placed at the exit of the air tunnel. And the flow speed outputs were manually recorded. The results of the flow speed data collection for water and air are shown in Figures 3 and 4, respectively. In Figure 3, it can be seen that as the pump frequency was increased, the average flow speed linearly increased. In contrast, for Figure 4, as the knob position was increased, the average flow speed did not linearly increase. When the knob positions are above 9, the speed was not increased as steep as when knob positions are lower than 9. This nonlinearity can be attributed to weakness in the simple design of the custom-made air tunnel. The straight contracting cone design may fail to bring the full amount of high flowrate into the observation chamber. On the other hand, the diffuser at the end of the observation chamber may result in the back flow of the trailing turbulence air exiting the chamber [18].

This relationship allows the observer to correlate the controllable pump frequency and knob position to the average speed of the fluid during the experimentation.

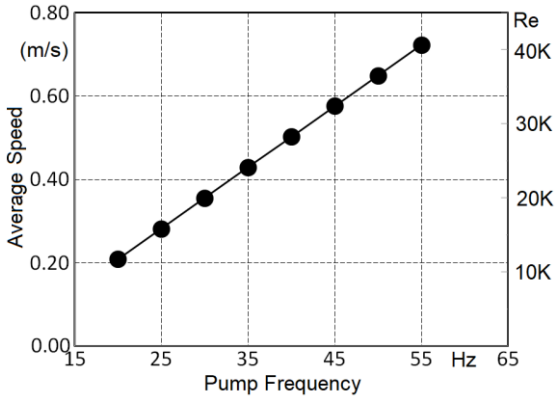


*Figure 3. Relation between pump frequency to the average flow speed (left axis) and its corresponding Reynolds numbers (right axis) for water.*

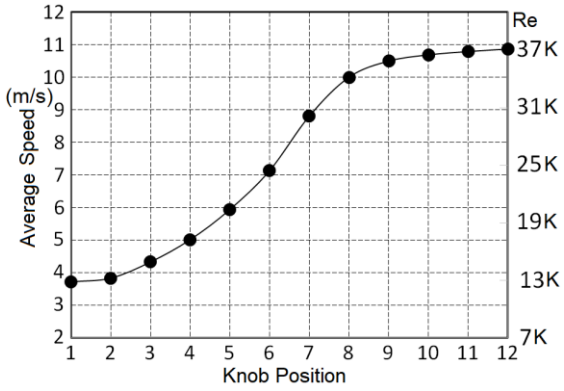


*Figure 4. Relation between knob position to the average flow speed (left axis) and its corresponding Reynolds numbers (right axis) for air.*

Inspiration for comparing the power output across different fluids came from testing for revolutions per minute (RPM) measurements in the custom air tunnel (see Figure 2). Initial research was conducted to observe how varying the diameter and infill density of the dual-cylinder turbine would affect pure rotation. For this experiment, only the turbine would rotate about its own axis, while the axle would remain fixed in its place. Figure 5 shows the measured RPM for the turbine exposed to varying air flow. At a Reynolds number of 30 K, the turbine began autorotating. This Reynolds number was therefore classified as a critical Reynolds number. The two data points to the left of the 30 K RPM value in Figure 5 represent data points during which the turbine did not experience any movement. As the Reynolds number increased, the RPM of the turbine increased as well, albeit in a non-linear trend.

Through monitoring the turbine during the RPM testing, it was observed that the turbine was relatively motionless at 13 K < Re < 18 K, demonstrated twisting and wiggling at 19 K < Re < 29 K, and experienced full autorotation at Re > 30 K. In Figure 5, data for Reynolds numbers below 20 K were excluded. The two filled-in dots represent data where the turbine would only twist and wiggle, while the empty dots reflect that the turbine continuously rotated. It can be concluded here that the critical Reynolds numbers associated with the initial autorotation occurring are at Reynolds numbers approximately between 25 and 30 K.

Despite initial belief that the flowing air would not generate enough inertia to rotate the turbine, encouraging test results showed that at certain Reynolds numbers of 25 K and above, the turbines generated significant RPM measurements. While rotating the turbine for power as opposed to freely rotating about its central axis would require more effort based on overcoming the turbine's inertia as well as the friction-tight bond between the turbine and the axle, a potential for comparison across differing fluids was deemed possible.

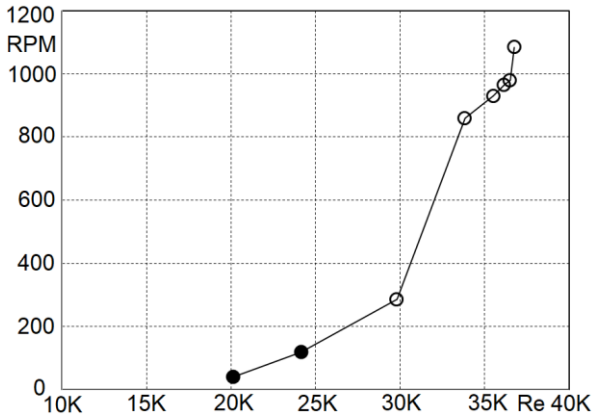


*Figure 5. RPM vs Reynolds number for turbine exposed to air flow. Filled circles indicate data of oscillating turbines. The turbines are in stagnation when the Reynolds numbers are less than 20 K. Exact critical Reynolds numbers require further experimentation.*

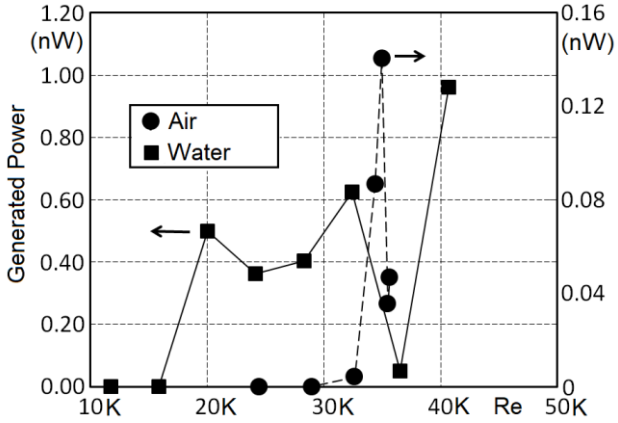


*Figure 6. Maximum power vs Reynolds number for turbine undergoing water flow (filled square – left axis) and air flow (filled circle – right axis)*

Figure 6 represents the calculated average power generated from the flowing water and air, which are represented by filled squares and filled circles, respectively. Note that the scales for power generated by water (on the left axis) is seven times much higher than that of air, which corresponds to the left and right axes, respectively. For the experiments involving power generation, the turbine shaft is coupled with the motor shaft using a rigid plastic tubing. The DC motor must be secured from water using a 3D-printed plastic case as shown in Figure 1. Both results from water and air indicate an increasing power production with respect to the increase in Reynolds numbers. Nevertheless, it was observed that there is a significant drop at Reynolds numbers between 30 K and 40 K that warrant further investigations. Interestingly, the drop for both cases, water and air, occur at a similar regime. Also noticed, as is expected, that both water and air demonstrate critical Reynolds numbers associated with the initial rotation modes. The critical Reynolds numbers, however, are different for these two fluids. The trend of increasing power with Reynolds numbers for a similar cross cylinder turbine design but performed in different flow tank was reported by Araneo [19].

Figures 7 and 8 show the time-averaged current and voltage, respectively, of the flowing water and air. The average voltage and current data were separately measured

and combined to produce the calculated power shown in Figure 6.

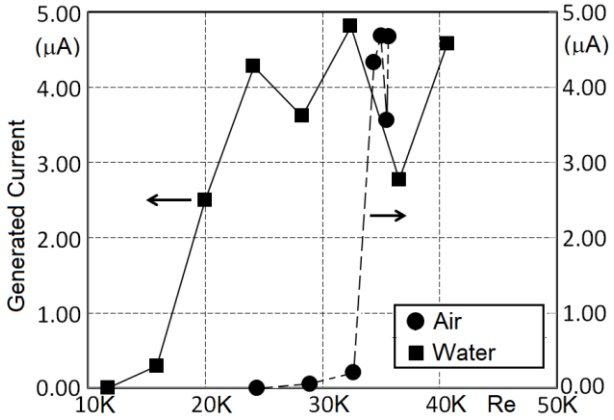


*Figure 7. Time-averaged current from the power experiments using water (filled square – left axis) and air (filed circle – right axis) versus Reynolds numbers on the horizontal axis.*

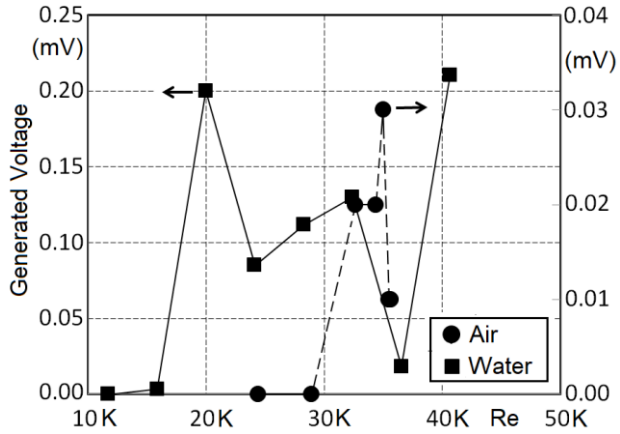


*Figure 8. Time-averaged voltage from the power experiments using water (filled square – left axis) and air (filed circle – right axis) versus Reynolds numbers*

From the plots shown in Figures 7 and 8, there is very little correlation between water and air in response to the increasing Reynolds number. Two such instances where water and air experienced the same trend occurred when the average current increased as the Reynolds numbers increased from 28 K to 33 K and when the voltage decreased from 33 K to 38 K. While correlations across both fluids are scarce, both plots in Figures 7 and 8 depict that there are critical Reynolds numbers associated with the current and voltage generations. Interestingly, the currents generated from both fluids was relatively equal. This indicates a possibility that current generation is independent of fluid density. The same could not be said for voltage. The voltage scale for water in Figure 8 on the left side is larger than the voltage scale for air on the right side by an approximate magnitude of five.

From the testing, it can be seen that despite the water having an average water flow speed less than that of air, the generated power is larger. For example, when the water velocity is 0.5 m/s ($Re \approx 28\ K$), which is drastically smaller than the average air flow speed of 10.6 m/s ($Re \approx 35\ K$), the power generated from the same turbine was larger in water by a factor of approximately three (3) when compared to air. This is certainly attributed to the density ratio between the two fluids. As previously stated, the density of water is 998 kg/m3, a massive value compared to 1.225 kg/m3 for the density of air. Because the volumes of the two chambers are relatively similar, the energy generated in both chambers would be different. This can be explained using the ratio of kinetic energy produced by the two fluids. Assuming that the generator maintains its efficiency $\eta$, the energy per unit volume generated by the air can be estimated as $w_a \approx \eta \frac{\rho_a \bar{V}_a^{\,2}}{2}$. Similarly, the energy per unit volume by the water is $w_w \approx \eta \frac{\rho_w \bar{V}_w^2}{2}$, for which $\rho_w = \frac{998}{1.2}\rho_a = 831\rho_a$ and, for the example given above, the water velocity $\bar{V}_w = \frac{0.5}{10.6} = 0.047\ \bar{V}_a$. Hence, $w_w \approx \eta \frac{831\ \rho_a \times 0.0022\ \bar{V}_a^2}{2} = 1.83\ w_a$, which is slightly less than 3. For different velocity ratios, the power and energy ratios certainly will be different. Also note that, while the current measurements were comparable across both fluids, the voltage saw substantial differentiation. As voltage is defined as the amount of potential energy available or work done per unit charge, the more stored energy present in the system, the greater the voltage. The effects of the fluid density on the current and voltage output by this turbine require further investigation. Nevertheless, theoretically, because water has a heavier mass than air for the same volume, when operated at the same speed, water will produce larger power generated when compared to air.

Figures 7 and 8 show that a peak of voltage and current occur at a Reynolds number of approximately 32 K, followed by a significant decrease at a Reynolds number of around 36 K. This peculiar phenomenon seems to be independent of fluid type as it happens to both fluids. This result could be attributed to the specific choice of the geometry, the density of the turbine being studied, and the blockage ratio, defined as the ratio of channel width to the turbine diameter. A two-dimensional computer simulation study on flowing fluid past a cylinder showed that blockage ratios affects the drag and lift coefficient [20]. Many other factors that can be considered in the drop of power generation include the change of flow complexity for the corresponding Reynolds numbers, possible bending of the turbine shaft, and friction caused from the bearings. The flow streamlines in the observation chamber were designed to be ideally uniform, but at high Reynolds numbers this condition might not have been achieved in real experimentation. Nevertheless, a rebound in power was seen for the water experiment at a Reynolds number of around 40 K. Similar data for air are not available due to the weakness in the air tunnel design. Further investigation should be performed with a finer increment of Reynolds numbers to better understand the trend in these regimes.

## IV. Conclusion

Autorotation of bladeless turbines is a complex study due to various fluid dynamic parameters that take place. In this project, the results generally indicate an increase in the power generation with the increase of the Reynolds numbers, at least for the given range. The current data also indicates existence of critical Reynolds numbers that have yet to be specifically determined. When factoring in complex flow distribution from the flow source, leakage throughout the air tunnel, and minimal power generation due to the small geometrical scales, precise conclusions about applying bladeless turbines to large scale applications cannot be confirmed in this paper. For the same turbine submerged in a similar volume, air yielded inferior power generation compared to water. The density of the flowing water harnesses more mechanical energy than air,

The project was funded by SUNY New Paltz Summer Undergraduate Research Program (SURE) award for Seth Pearl. The design and fabrication of the water tank was sponsored by the Vibration Institute. The design and fabrication of the air tunnel was sponsored by the Mechanical Engineering Program of SUNY New Paltz.

which results in more electrical energy generated. Additionally, having a larger fluid flow speed does not always correlate to more turbine rotations. There are many factors that contribute to power generation from hydrokinetic energy, and this experiment showed that despite water having a significantly lower flow speed, it yielded more power generation than air.

## REFERENCES


[1] "Renewable energy | Definition of Renewable energy at Dictionary.com.".Available: https://www.dictionary.com/browse/renewable-energy. [Accessed: 19-Mar-2020].

[2] K. Ismail, T. Batalha, and F. Lino, "Hydrokinetc turbines for electricity generation in isolated areas in the Brazilian Amazon," Int. J. Eng. Tech. Res., vol. 3, pp. 127–135, 2015.

[3] L. I. Lago, F. L. Ponta, and L. Chen, "Advances and trends in hydrokinetic turbine systems," Energy Sustain. Dev., vol. 14, no. 4, pp. 287–296, 2010.

[4] M. Sood and S. K. Singal, "Development of hydrokinetic energy technology: A review," Int. J. Energy Res., vol. 43, no. 11, pp. 5552–5571, 2019.

[5] M. J. Khan, G. Bhuyan, T. Iqbal, J. E. Quaicoe, M. T. Iqbal, and J. E. Quaicoe, "Hydrokinetic Energy Conversion Systems and Assessment of Horizontal and Vertical Axis Turbines for River and Tidal Applications: A Technology Status Review," Appl. Energy, vol. 86, no. 10, pp. 1823–1835, Oct. 2009.

[6] H. Anuta, P. Ralon, M. Taylor, and F. La Camera, "Renewable power generation costs in 2018," Int. Renew. Energy Agency, Abu Dhabi, 2019.

[7] H. J. Lugt, "Autorotation," Annu. Rev. Fluid Mech., vol. 15, no. 1, pp. 123–147, Jan. 1983, doi: 10.1146/annurev.fl.15.010183.001011.

[8] B. W. Skews, "Autorotation of many-sided bodies in an airstream," Nature, vol. 352, no. 6335, pp. 512–513, 1991.

[9] R. Camassa, B. Chung, P. Howard, R. McLaughlin, and A. Vaidya, "Vortex induced oscillations of cylinders at low and intermediate Reynolds numbers." Springer, pp. 135–145, 2010.

[10] J. Araneo, B. J. Chung, M. Cristaldi, J. Pateras, A. Vaidya, and R. Wulandana, "Experimental control from wake induced autorotation with applications to energy harvesting," Int. J. Green Energy, vol. 16, no. 15, pp. 1400–1413, Dec. 2019.

[11] I.-B. Lee and S. Park, "Improving Tube Design of a Problematic Heat Exchanger for Enhanced Safety at Minimal Costs," Energies, vol. 10, p. 1236, 2017.

[12] N. A. Saadabad, H. Moradi, and G. Vossoughi, "Semi-active control of forced oscillations in power transmission lines via optimum tuneable vibration absorbers: With review on linear dynamic aspects," Int. J. Mech. Sci., vol. 87, pp. 163–178, 2014, doi: https://doi.org/10.1016/j.ijmecsci.2014.06.006.

[13] P. D'Asdia and S. Noè, "Vortex induced vibration of reinforced concrete chimneys: in situ experimentation and numerical previsions," J. Wind Eng. Ind. Aerodyn., vol. 74–76, pp. 765–776, 1998.

[14] J. D. Holmes, B. L. Schafer, and R. W. Banks, "Wind-induced vibration of a large broadcasting tower," J. Wind Eng. Ind. Aerodyn., vol. 43, no. 1, pp. 2101–2109, 1992, doi: https://doi.org/10.1016/0167-6105(92)90640-V.

[15] B. MM, R. K, B.-S. YY, and G. EM., "VIVACE (Vortex Induced Vibration Aquatic Clean Energy): A New Concept in Generation of Clean and Renewable Energy From Fluid Flow," ASME. J. Offshore Mech. Arct. Eng., vol. 130, no. 4, pp. 41101–41115, 2008.

[16] V. Sivadas and A. M. Wickenheiser, "Small-scale wind energy harvesting from flow-induced vibrations," in Smart Materials, Adaptive Structures and Intelligent Systems, 2011, vol. 54716, pp. 737–744.

[17] H. D. Akaydin, N. Elvin, and Y. Andreopoulos, "Energy harvesting from highly unsteady fluid flows using piezoelectric materials," J. Intell. Mater. Syst. Struct., vol. 21, no. 13, pp. 1263–1278, 2010.

[18] C. Hodanbosi, "The Wandering Wind Tunnel," 2014. [Online]. Available: https://www.grc.nasa.gov/www/k-12/WindTunnel/wandering_windtunnel.html.

[19] J. Araneo, B. J. Chung, M. Cristaldi, J. Pateras, A. Vaidya, and R. Wulandana, "Experimental control from wake induced autorotation with applications to energy harvesting," Int. J. Green Energy, vol. 16, no. 15, pp. 1400–1413, Dec. 2019,.

[20] S. Singha and K. P. Sinhamahapatra, "Flow past a circular cylinder between parallel walls at low Reynolds numbers," Ocean Eng., vol. 37, no. 8–9, pp. 757–769, 2010.